HHS Public Access

Author manuscript

Phys Med Biol. Author manuscript; available in PMC 2019 March 21.

Published in final edited form as:

Phys Med Biol. ; 63(6): 064002. doi:10.1088/1361-6560/aab241.

In vivo optoacoustic temperature imaging for image-guided cryotherapy of prostate cancer

E.V. Petrova[1,a], **H.P. Brecht**[1,b], **M. Motamedi**[2], **A.A. Oraevsky**[1,c,*], and **S.A. Ermilov**[1,b]

[1]Tomowave Laboratories, Inc, 6550 Mapleridge St, Ste 124, Houston, Texas 77081-4629

[2]The University of Texas Medical Branch at Galveston, 301 University Blvd, Galveston, Texas, 77555

Abstract

The objective of this study is to demonstrate *in vivo* the feasibility of optoacoustic temperature imaging during cryotherapy of prostate cancer. We developed a preclinical prototype of optoacoustic temperature imager that included pulsed optical excitation at 805-nm wavelength, a modified clinical transrectal ultrasound probe, parallel data acquisition system, image processing and visualization software. Cryotherapy of a canine prostate was performed *in vivo* using a commercial clinical system Cryocare® CS with an integrated ultrasound imaging. The universal temperature-dependent optoacoustic response of blood was employed to convert reconstructed optoacoustic images to temperature maps. Optoacoustic imaging of temperature during prostate cryotherapy was performed in the longitudinal view for the region of 30 mm (long) × 10 mm (deep) that covered the rectum, Denonvilliers fascia, and posterior portion of the treated gland. The transrectal optoacoustic images showed high-contrast vascularized regions, which were used for quantitative estimation of local temperature profiles. The constructed temperature maps and their temporal dynamics were consistent with the arrangement of the cryoprobe and readouts of the thermal needle sensors. The temporal profiles of the readouts from the thermal needle sensors and the temporal profile estimated from the normalized optoacoustic intensity of the selected vascularized region showed significant resemblance, except for the initial overshoot that may be explained as a result of the physiological thermoregulatory compensation. The temperature was mapped with errors not exceeding ±2°C (St.Dev.) consistent with the clinical requirements for monitoring cryotherapy of the prostate. *In vivo* results showed that the optoacoustic temperature imaging is a promising non-invasive technique for real-time imaging of tissue temperature during cryotherapy of prostate cancer, which can be combined with the transrectal ultrasound – the current standard for guiding clinical cryotherapy procedure.

Keywords

optoacoustic tomography; photoacoustic imaging; temperature monitoring; thermal therapy; cryoablation

[*]Corresponding author: AAO@tomowave.com, phone: (713) 270-5393.

[a]**Present affiliation:** Department of Medicine, Baylor College of Medicine, 1 Baylor Plaza, Houston, Texas 77030

[b]**Present affiliation:** PhotoSound Technologies, Inc, 5658 Sylmar Rd, Houston, Texas, 77081

[c]**Present affiliation:** Translational Medical Center for Minimally Invasive Technologies, Fifth Affiliated Hospital, Guangzhou Medical University, 621 Gangwan Rd, Guangzhou City, China, 510700.

Introduction

Prostate cancer is recognized as one of the most prevalent malignant diseases and is the third most diagnosed cancer in the United States following the breast and the lung cancers (Howlader *et al.*, 2017). The National Cancer Institute (USA) estimates that during 2017, approximately 161,000 new cases of prostate cancer will be diagnosed, and 27,000 men will die of this disease in the United States (Howlader *et al.*, 2017). Two major forms of treatment for patients with localized prostate cancer are surgery and radiation therapy, have been associated with significant complications and risks, including urinary incontinence, bowel symptoms, and impotence (Garnick, 1993). Therefore, there has been a continuous search for alternative procedures, and one of the most promising is cryotherapy, also called cryosurgery or cryotherapy (Rukstalis and Katz, 2007; Mohammed *et al.*, 2014).

Cryotherapy is a minimally-invasive clinical technique for primary and/or salvage treatment of prostate cancer, which is performed as a same-day outpatient procedure with fast (2-3 days) recovery (Rukstalis and Katz, 2007; Bjerklund Johansen *et al.*, 2013; Mohammed *et al.*, 2014). A patient also benefits from a low toxicity profile, minimal anesthesia (can be performed with a spinal block), and low cost (less than half as compared to conventional eradicative surgical procedures or radiation therapy) (Roberts *et al.*, 2011; Resnick *et al.*, 2013). Cryotherapy of prostate cancer is used as a primary treatment technique or as a secondary (salvage) treatment for those patients who exhibited a recurrence of cancer following the primary radiation treatment – 30% according to some studies (Agarwal *et al.*, 2008). The aspects of minimal invasiveness and good cancer control make it a reasonable option for many men. However, the clinical efficacy of cryotherapy is undermined by frequent overtreatment of neighboring healthy tissues and organs during alternating cycles of deep freezing and thawing (Chu and Dupuy, 2014).

The standard clinical procedure for cryotherapy of prostate cancer, approved by the U.S. Food and Drug Administration (FDA), involves the following steps (Rukstalis and Katz, 2007). First, the surgeon positions a transrectal ultrasound probe and captures key reference images in transverse and sagittal sections of the prostate. Next, according to the prostate geometry and suspected or known location of the lesion, the surgeon inserts transperineally 5-7 cryoprobes, each 1.5-3 mm in diameter, while monitoring cryoprobe positioning with the ultrasound. In the third generation of cryotherapy systems, which is currently employed in clinical practice, pressurized argon gas is cooled below −100°C inside the cryoprobes via Joule-Thomson effect freezing tissues surrounding the exposed tip of a cryoprobe within seconds (Maytal, 1998). The cryoprobes are set at a safe distance (not less than 5 mm) from the vulnerable structures of the urethra and rectal wall and the lengths of their freezing tips are adjusted to cover precisely only the treated area. Two or three thermal sensors are inserted near the lesion, the urethra, and the rectal wall. The surgeon inserts a urethral warming catheter with circulated saline, helping a patient to maintain urinary function. The first freezing cycle is activated until the thermal sensor positioned near the lesion starts showing targeted lethal temperatures below −40°C. At the same time, the ultrasound image is monitored to assure that the expanding iceball does not reach the rectal wall. After the targeted low temperatures are achieved (5-10 minutes), the cryosystem is switched into the

active thawing cycle by circulating Helium inside the cryoprobes. The active thawing cycle continues until all the thermal sensors display temperatures above 0°C. Then, the freezing cycle is repeated again. Eventually, the prostate is allowed to slowly thaw by simply turning off the circulation of Argon inside the cryoprobes.

The precise control of cryotherapy is crucial for both successful destruction of malignancies and minimization of the damage to adjacent healthy tissues. The temperature level of 0°C is of particular importance since it is associated with potential vascular damage and apoptosis of healthy non-frozen tissues (Theodorescu, 2004; Robilotto *et al.*, 2013) (Figure 1). Mapping this isotherm over the ultrasound image of the prostate in real-time would provide an extremely valuable feedback for the surgeon. The temperature accuracy of ±5°C is considered sufficient by many urologists to warrant the effective destruction of malignancies while preventing damage to important healthy tissues (Mohammed *et al.*, 2014).

The current routine clinical practice of cryotherapy relies on few discrete temperature readouts provided by thermal needle sensors, which are inserted directly into the treated prostate and nearby tissues (external sphincter of the urethra and Denonvilliers fascia separating the prostate and the rectum). Additional control is provided by continuous monitoring of the leading edge of the forming ice ball and its position with respect to the rectal wall using transrectal ultrasound imaging (Rukstalis and Katz, 2007). However, ultrasound image provides an estimate only on the extent of the direct tissue damage by visualizing boundary of the ice ball corresponding to about −20°C (Hsiao and Deng, 2016). The fact that ultrasound can only track the leading edge of the ice ball and the sparse distribution of temperature readout points within extreme temperature gradients significantly reduces capabilities of the surgeon to evaluate tissue damage induced by the ongoing cryotherapy. Those limitations on direct thermal monitoring during cryotherapy of prostate cancer contribute to a set of complications including impotence (85-95%), incontinence (5-40%), and more severe thermal damage of rectum (up to 2%) requiring additional surgical intervention (Ismail *et al.*, 2007; Jones *et al.*, 2008; Williams *et al.*, 2011). In order to improve the clinical safety of cryotherapy and to reduce the occurrence of the side effects caused by irreversible thermal damage to the healthy tissues, accurate temperature maps have to be obtained from the entire treated area and its neighborhood in real time.

An ideal image-guiding component of the cryotherapy system should provide real-time visualization of the temperature changes in the treated tissue, be compatible with the used therapeutic equipment, convenient in operation, and should not drive the cost of the entire instrument prohibiting its clinical use. Optoacoustic tomography (OAT) was previously proposed for real-time temperature imaging of live vascularized tissue (Petrova *et al.*, 2014; Petrova *et al.*, 2016). OAT is a method that combines pulsed optical excitation of live tissue and ultrasound detection of the generated pressure waves to overcome resolution limits imposed by light scattering (Wang and Hu, 2012; Oraevsky, 2014). Optoacoustic (OA) detection could be performed by a clinical ultrasound probe modified for a light-triggered receive mode (Fronheiser *et al.*, 2010; Yaseen *et al.*, 2010; Jaeger *et al.*, 2013). OAT performed with NIR excitation enables interrogation of tissues that can be at a depth of several centimeters (Wang and Hu, 2012; Oraevsky, 2014). OAT systems are substantially less expensive alternatives to magnetic resonance (MR) temperature imaging modalities,

compatible with conventional clinical transrectal ultrasound, and have been used in clinical research for applications related to cancer detection, including breast cancer (Neuschler *et al.*, 2017) and prostate cancer (Yaseen *et al.*, 2010).

Almost two decades ago, it was established that optoacoustic signals significantly change in magnitude if the interrogated biological tissues are heated or cooled (Esenaliev *et al.*, 1999; Larin *et al.*, 2000; Esenaliev *et al.*, 2000). The effect was explained by the temperature dependence of thermoacoustic efficiency (Grüneisen parameter) contributing to optoacoustic effect (Nikitin *et al.*, 2012). Consequently, when the local temperature is changing, the amplitude of the measured OA response, generated in that particular locality, replicates in a linear fashion the behavior of the Grüneisen parameter, which constitutes the fundamental concept of OA temperature monitoring (Larina *et al.*, 2005). Optoacoustic thermometry was extensively studied in tissue phantoms and in biological samples (Pramanik and Wang, 2009; Soroushian *et al.*, 2010; Wang and Emelianov, 2011; Nikitin *et al.*, 2012; Chen *et al.*, 2013; Ke *et al.*, 2014). Our group presented a more accurate approach for optoacoustic thermometry by reconstruction of 2D temperature images (Petrova *et al.*, 2013, 2014, 2016) that can be used during cryotherapy of vascularized tissues. Using blood samples and tissue mimicking phantoms we demonstrated that optoacoustic temperature imaging (OA-Tim) can be performed in vascularized tissues due to the exclusive compartmentalization of optically absorbing molecules of hemoglobin inside red blood cells (Petrova *et al.*, 2014; Petrova *et al.*, 2016). Such spatial segregation of the dominant optical absorber inside stable cytoplasmic environment makes red blood cell a universal endogenous optoacoustic temperature sensor. As a result, identical temperature-dependent optoacoustic response (ThOR) can be observed in all types of vascularized tissues regardless of the bulk tissue composition. The ThOR of blood obtained while irradiating samples with 805-nm laser pulses was found independent of blood oxygen saturation and hematocrit (Petrova *et al.*, 2014; Petrova *et al.*, 2016). Therefore, the proposed temperature imaging technique should be applicable for thermal interrogation of both microvasculature and systemic blood vessels carrying venal or arterial blood. We also established a procedure providing accurate conversion of optoacoustic images of vascularized tissues to the temperature maps (Petrova *et al.*, 2016). The procedure was validated in tissue-mimicking phantoms for the clinically relevant range of temperatures, spatial temperature gradients, and time-frames typical for cryotherapy. We demonstrated that OA temperature imaging can non-invasively map isotherms that are relevant for cryotherapy of prostate cancer at a frame rate of 1 fps (frames-per-second) and with single readout accuracy as good as ±1 °C.

The objective of these studies was to demonstrate for the first time optoacoustic temperature imaging in non-frozen tissue during cryotherapy of prostate using *in vivo* canine model. A prototype OA imaging unit, employed for that task integrated pulsed optoacoustic excitation at 805-nm wavelength, a clinical transrectal ultrasound probe, parallel data acquisition (DAQ) system, and image processing and visualization software enabling real-time visualization of 2D temperature maps of the rectal wall, Denonvilliers fascia, and posterior regions of prostate – the areas, which are most critical to keep intact during cryotherapy of prostate cancer.

Materials and Methods

Optoacoustic imaging of temperature during cryotherapy of prostate

Optoacoustic imaging of temperature during cryotherapy of a canine prostate was performed in the sagittal (longitudinal) view for the region of 30 mm (long) × 10 mm (deep) that covered the rectum, Denonvilliers fascia, and posterior portion of the treated gland. Such technique could be potentially used in clinical practice to assure that permanent thermal damage does not extend to the important neurovascular regions and the rectum. The monitored tissues are well vascularized. Therefore, for temperature imaging, we employed the previously developed method utilizing a reference OA frame at the known temperature just prior to initiation of cryotherapy (Petrova *et al.*, 2016). The temperature imaging procedure included two steps: (1) obtain the OA reference frame including the region of interest (ROI) at a known temperature prior to cryotherapy, (2) normalize subsequent OA frames to the reference frame and use the calibration equation for the optoacoustic temperature imaging (OA-Tim) obtained for blood to convert each normalized frame to the temperature map. The method showed *in vitro* accuracy as high as ±1°C for temperatures below 0°C and average accuracy of ±3°C for the entire interrogated range of temperatures between 40°C and −16°C (Petrova *et al.*, 2016).

A general equation for normalized ThOR includes two material-specific parameters T_0 and ΔT_{max} allowing experimental image data to be fitted with a second-order polynomial function (Petrova *et al.*, 2014).

$$\overline{OA} = -\frac{4\Delta T_{max}}{(T_1 - T_0)^3}(T - T_0)(T - T_1) + \frac{T - T_0}{T_1 - T_0} \quad (1)$$

Where $\overline{OA}$ is the normalized optoacoustic intensity; T – temperature (°C), T_1 – normalization temperature prior to cryotherapy, ($\overline{OA}(T_1) \equiv 1$). T_0 is the temperature of zero optoacoustic response; ΔT_{max} is the maximum thermal nonlinearity of ThOR in the temperature range [T_0 T_1]. For the samples of porcine blood we found T_0 = −13.8±0.1°C and ΔT_{max} = 11.4±0.1°C at T_1 = 37°C (Petrova *et al.*, 2016). Laser wavelength of 805 nm was used for excitation of OA response.

The design of the OA-Tim unit was based on minimal modifications to the FDA-approved and well-established TRUS-guided systems for the cryotherapy of prostate cancer (Zisman *et al.*, 2001). The prototype of OA-Tim unit utilized core technology of the laser optoacoustic imaging system (LOIS, TomoWave Laboratories, Inc., Houston, Texas). Its schematic is shown in Figure 2(a). A pulsed Ti-Sapphire laser (Spectra Wave, TomoWave Laboratories, Houston, TX) was tuned to the isosbestic point of hemoglobin at 805 nm and produced 6 ns, 30 mJ per pulse laser radiation with pulse repetition rate of 10 Hz. Parallel 128-channel OA data acquisition was triggered on every pulse of the excitation laser allowing 10 frames per second imaging. For each frame, 1024 samples per channel were acquired at 25 MHz sampling rate and transferred over the Ethernet interface to a personal

computer (PC) for real-time OA reconstruction, visualization, and post-processing of the temperature maps.

Optoacoustic temperature imaging unit required integration of the fiberoptic bundles into the transrectal ultrasound probe in order to enable a reflection-mode OA configuration for imaging prostate and neighboring tissues. In the OA backward mode, the distribution of optical fluence in tissue is minimally affected by the ice ball forming in the far field. We used Monte Carlo computer simulation of light distribution and OA detection in a prostate with the proposed TRUS configuration (Ermilov *et al.*, 2009) to optimize the arrangement of the output fiberoptic apertures. A clinical transrectal ultrasound probe (ER7B, Acuson, CA) with the center frequency of 6 MHz was upgraded with fiberoptic illumination according to the results of the MC simulations enabling optoacoustic imaging of a prostate in the longitudinal view. The cylindrical surface of the probe was cut flat on both sides of the longitudinal linear array of transducers. A randomized fiberoptic bundle was fabricated with the output terminal shaped in a U-profile that fit tightly around the working end of the ultrasound probe. Such design enabled two 2mm × 30mm rectangular light-emitting apertures arranged on both sides of the longitudinal array of the probe separated by a distance of 20 mm (Figure 2(b)). The length of each light-emitting aperture (and consequently the field of view) was limited to 30 mm in order to accommodate the requirements for ½ inch diameter of the fiberoptic input, coupled to the open beam of the laser.

Canine prostate model

In vivo evaluation of the OA temperature imaging was performed by monitoring cryotherapy of a canine prostate. A canine model of prostate cancer has been commonly accepted by academic researchers in the USA, since the dog's prostate shares many anatomical similarities to that of a human (Fonseca-Alves *et al.*, 2013). In our studies, an animal with normal prostate was studied to demonstrate the feasibility of the OA temperature imaging technique. The animal was male mongrel 5 years of age, weighing 9.2 kg. The experiments were performed according to the IACUC protocol approved by the University of Texas Medical Branch at Galveston (UTMB). Prior to the imaging procedure, the animal was housed and cared for in the Animal Research Center of UTMB with professional veterinarians on duty 24 hours a day. No special services for animal care and housing were required.

In vivo imaging procedure and data analysis

Cryotherapy of the canine prostate was performed using the commercial clinical system Cryocare® CS (Healthtronics, Austin, Texas) with integrated ultrasound imaging. Laser safety standards were assured by operating at a pulse energy level of 30 mJ split between two fiberoptic illuminators having a total attenuation of 50% each. The resulting laser fluence at the output of the probe was limited to 12.5 mJ/cm^2, which is below the safe level of laser irradiation of human skin recommended by the American National Standards Institute (ANSI, 2007).

Prior to cryotherapy, a dog was administered with the pre-anesthesia drug combination of 0.25 mg/lb Promace, 0.02 cc/kg Torbugesic and 0.25 mg/lb Atropine (all IM). The anesthesia was performed with 20 mg/kg Pentothal IV and 0.5-2% Halothane, administered to effect as needed. The canine subject was fully anesthetized during cryotherapy.

The anesthetized dog was rested on an animal surgery bed in the supine position. The prostate was located, its outline and the urethra were mapped in both longitudinal and transverse views using the transrectal ultrasound (TRUS) of Cryocare® CS. The ultrasound probe was fixed in the probe holder with the CryoGrid™ fixture that allowed precise positioning of the cryoneedle and the temperature sensors. A single cryoneedle was inserted into the bulk of the prostate near and just below the urethra. Three temperature sensors were inserted into and nearby the prostate to provide direct reference temperature readings. The positioning of the needles was guided by the transrectal ultrasound. The temperature sensors, which were monitoring areas near the rectum, were placed away from the longitudinal imaging plane in order to minimize OA imaging artifacts.

The ultrasound probe was removed and the OA-Tim probe was inserted into the rectum of the animal to the same position as the ultrasound probe using the quick-latch advantages of the Cryocare® CS probe holder. A single freezing event was performed for 3 minutes 30 seconds while continuously recording averaged optoacoustic data at a rate of 2 frames per second (Figure 3). The recording was continued after the freezing for 1 minute 20 seconds to observe changes associated with the passive thawing. The OA-Tim probe was removed and the Cryocare® CS TRUS probe was inserted again to verify the formation of the ice ball.

Following the cryotherapy and imaging, euthanasia of the animal was performed by intravenous injection of 20 cc of potassium chloride solution, consistent with the recommendations of the Panel on Euthanasia of the American Veterinary Medical Association. The death of the animal was assured by open-chest examination. Following euthanasia, the prostate of the test animal was removed, dissected, and examined to verify thermally induced damage.

The OA data was processed offline using the proprietary Matlab-based software. The OA data and temperatures recorded by needle sensors were time stamped with respect to the internal PC clock for subsequent synchronization. Individual OA frames were reconstructed using the filtered back-projection algorithm (Kruger *et al.*, 1995) modified to include impulse response of ultrasonic transducers. Non-invasive OA-Tim was performed in selected high-intensity parts of the OA image (containing blood vessels) using median statistical estimate in a manually selected ROI. Previously, we demonstrated in phantoms that such method of image-analysis enables high-precision quantification of the local OA response (Petrova *et al.*, 2013). The speed of sound was adjusted for individual frames to minimize defocusing of the OA images caused by the thermal changes in the treated tissues. The algorithm employed correlation of each OA frame, reconstructed using the various speed of sound values, with the reference ROI OA image. The speed of sound that provided the highest maximum across all the correlation matrices was used for the reconstruction of that particular OA frame (Petrova *et al.*, 2016).

The algorithm for OA-Tim was implemented as follows:

1. (1) The parameters of the calibration curve T_1, T_0 and $\Delta T_{max}(T_1)$ (Eq. 1), which are applicable for the processed dataset, were selected. For the *in vivo* canine prostate cryotherapy: T_1 = 35°C – the average temperature measured by the control thermal needle sensors prior to cryotherapy; Two other calibration parameters were selected from the ThOR of blood previously evaluated *in vitro* (Petrova *et al.*, 2016): T_0 = −13.8 °C and ΔT_{max}(35°C) = 10.2 °C recalculated for $T_{1(2)}$ = 35°C from $T_{1(1)}$ = 37°C and ΔT_{max}(37°C) = 11.4 °C using the formula

$$\Delta T_{max}(T_{1(2)}) = \frac{\Delta T_{max}(T_{1(1)})(T_{1(2)} - T_0)^2}{-4\Delta T_{max}(T_{1(1)})(T_{1(2)} - T_{1(1)}) + (T_{1(1)} - T_0)^2} \quad (2)$$

   Selection of a new T_1 forced recalculation of ΔT_{max}.

2. A number of the reference OA frames to be acquired at the initial temperature T_1 was selected. The reference frames were averaged to reduce the noise. We also set: the image smoothing kernel, visualization (image brightness) threshold, and transparency of the temperature image, which was superimposed on the optoacoustic grayscale image. The temperature threshold was expressed in percent of the dynamic range of the reference frame. The brightness values on the temperature image, which were below the noise level, were not used in the temperature imaging. The T-map was made transparent at those locations so that only grayscale optoacoustic image was visible. The *transparency* parameter sets constant transparency for the displayed temperature maps. The temperature maps presented in this work were processed with the following parameters: *temperature map threshold* 15% of the 8-bit dynamic range of a grayscale OA reference frame; *smoothing kernel* of 3 pixels; and *transparency* of 40%.

3. The reference OA frame was reconstructed.

4. Temperature maps were created by conversion of the ratio of the current frame to the reference frame using the temperature calibration curve and other parameters selected in the steps 1 and 2.

5. A color-coded temperature map was superimposed on the grayscale optoacoustic image of each frame with a user-set transparency. A linear grayscale palette was used for display of all optoacoustic images. The palette was autoscaled for the reference frame and the limits were fixed for all the subsequent frames.

Results

In vivo optoacoustic images were acquired prior, during, and post-cryotherapy of the prostate. The optoacoustic and temperature images presented in this work are oriented such that they can be overlaid on the longitudinal view of transrectal ultrasound.

Figure 4(a) shows a transverse ultrasound image and Figure 4(b) shows a longitudinal ultrasound image of the dog's prostate prior to cryotherapy. Prostate's cross section is 25 mm (anterior-posterior) × 30 mm (left-right). The cryoprobe and the thermal sensor #1 (Th1) are clearly visible on the transverse image inside the prostate at a depth of about 10 mm, just below the urethra (cryoprobe at 12 o'clock and Th1 at 11 o'clock inside the right lateral lobe). The rectal wall, which is about 2 mm thick, is also clearly visible in Figure 4(a). Th1 was set near the cryoprobe (about 2 mm away) and was used to guide the cryotherapy procedure. The freezing cycle was stopped after Th1 was consistently showing lethal temperatures below −40°C for 1 minute. Figure 4(b) shows two other thermal sensors (Th2 and Th3), which were set traversing Denonvilliers fascia on the left and on the right of the midsection plane at a distance of about 6-8 mm away from the cryoneedle. Those sensors were located at a similar distance from the cryoprobe as compared to vascularized regions of the rectal wall and Denonvilliers fascia, which were monitored using OA imaging technique. The temperature readouts from Th2 and Th3 were used for validation of the optoacoustic temperature readouts. The longitudinal view on Figure 4(b) also shows that the Th1 was set at an angle of about 10-20° with respect to the cryoprobe and two other sensors. The region, indicated on Figure 4(b) by the dashed red rectangle with dimensions of 22mm × 10mm, was used for OA imaging at 805-nm laser excitation wavelength and for construction of the OA temperature images (OA-Tim). The OA image shows high contrast regions of blood vessels, which were used for numerical evaluation of temperature profiles. A typical OA-Tim is shown for one of the OA frames prior to the initiation of freezing cycle (T_1 = 35°C).

We applied the OA-Tim procedure described in the Materials and Methods section to visualize the spatial distribution of the temperature as it was changing during cryotherapy (Figure 5). The freezing cycle of cryotherapy lasted for 3 min 35 sec. The passive thawing cycle was then monitored using OA-Tim for additional 1 min 25 sec.

Each OA-Tim frame also shows in pseudocolor the temperatures recorded simultaneously by the thermal sensors Th2 and Th3. The used color palette smoothly transitions over the RGB triplet for the temperature range [35, −20] °C, with 0°C coded by the cyan color. All the timestamps indicated on the images were set with respect to the beginning of the freezing cycle.

The constructed temperature distributions and their temporal dynamics are consistent with the arrangement of the cryoprobe and readouts of the thermal sensors. Figure 5(b) shows OA-Tim for: (1) a frame recorded at the end of the freezing cycle (top image, Time = 215 s), (2) a frame recorded in the beginning of the passive thawing cycle (middle image, Time = 225 s), and (3) a frame recorded when the thawing was ongoing for 1 min 15 s (bottom image, Time = 290 s). Figure 5(b) also shows two ultrasound images verifying the formation of the ice ball and showing its dynamics during the passive thawing cycle, with the time difference between the two frames equal to 135 s. At the time moment of 335 s or 2 minutes after the freezing was terminated, the formidable ice ball is still visible on the ultrasound image with its leading edge spreading all the way to the posterior boundaries of the prostate (about 7.5 mm deep from the ultrasound probe). At that time the thermal sensor readouts were −1°C – Th1, 0°C – Th2, and 2°C – Th3. 2 minutes and 15 seconds later, the ice ball visibly retracted and the anterior hypoechoic region showed some texture, indicating that

there is no more clear ice boundary present, but rather a gradual transition exists between the warming and still frozen regions of tissue. The thermal sensors at that time showed −0.5°C – Th1, 7.5°C – Th2, and 12.7°C – Th3.

To further validate the optoacoustic temperature monitoring technique *in vivo*, we selected a smaller region of interest on the visualized portions of the rectal wall and Denonvilliers fascia, containing a high-contrast object – a blood vessel or well-perfused tissue area (see the inset on the Figure 6(b)). The object's median intensity, normalized for the reference frames acquired at 35°C prior to the freezing cycle, was converted to the temperature using the universal blood calibration of ThOR (see (Petrova *et al.*, 2016) and the Materials and Methods section). To verify that the selected object is not an image artifact, but is, indeed, a portion of tissue with high blood content allowing reliable optoacoustic temperature monitoring, we validated the relationship of the estimated normalized OA intensity versus average temperature measured by the nearby Th2 and Th3 (Figure 6(a)) and plotted it on the same graph with the universal ThOR of blood (Figure 6(b)). The relationship for the selected object, albeit noisier (average deviation from the reference ThOR curve is 2°C), still follows well the blood's ThOR.

The temporal profiles of the readouts from the thermal sensors Th2 and Th3 and the temporal profile estimated from the normalized OA intensity of the selected blood vessel show significant resemblance, except for the high overshot in the normalized OA intensity (labeled as "Thermal regulation" on the Figure 6(b)) at the early stage (first 1 minute) of the freezing cycle, when the thermal probes were still reading constant initial temperature (Figure 6(c)). Figure 6(d) shows the dissected canine prostate that experienced the cryotherapy procedure performed in these studies. The prostate was sliced across the urethra allowing visual examination of the transverse sections. The perforation damage from the thermal sensor (Th1) is clearly visible. Since in these studies the cryoneedle was positioned very close to the urethra and no special protection (like a warming catheter) was implemented, the cryotherapy procedure resulted in melting and complete closure of the urethra, which is similar to the urethral slothing – a complication, which was frequently observed in the earlier versions of the clinical procedure performed with the 1st generation of cryotherapy equipment (Mohammed *et al.*, 2014).

Discussion

We developed a pre-clinical prototype of an optoacoustic imaging system for monitoring cryotherapy of prostate cancer. The device is based on the existing laser optoacoustic imaging system (LOIS) armed with a modified transrectal ultrasound detector probe, which can be used in both optoacoustic and ultrasound modes. At this stage, our hardware did not allow simultaneous or interleaved visualization of optoacoustic and ultrasound data. However, such imaging configurations currently exist and are used for both preclinical and clinical research (Harrison and Zemp, 2011; Neuschler *et al.*, 2017). A conventional TRUS monitoring of cryotherapy could be beneficially combined with simultaneous optoacoustic imaging that can be converted into the temperature maps. Such maps can be directly overlaid on top of the ultrasound images, a feature similar to that provided by the power Doppler, enabling real-time non-invasive temperature monitoring over the extended regions within the

field of view. Such simultaneous real-time ultrasound-optoacoustic imaging will also allow more accurate interpretation of the optoacoustic maps, which is a necessary step for clinical translation of the imaging modality.

The developed prototype of an OA-Tim system enabled imaging of the prostate in the longitudinal view only. The next step, which is a mandatory prerequisite for clinical translation of the developed technology, would be to enable optoacoustic monitoring for the transverse array of the probe. The transverse array of the TRUS bi-plane probe is exclusively used during setup and planning of the clinical cryotherapy procedure: imaging the prostate and urethra, guiding the cryoneedles and thermal sensors. The transverse ultrasound image is also frequently consulted during the freezing and thawing cycles to estimate the extent of the iceball, particularly, if the modern experimental procedure of focal cryotherapy is performed in an attempt to spare the neurovascular bundle – a structure responsible for the erectile function of a patient (Nguyen *et al.*, 2013; Durand *et al.*, 2014). There is no simple approach to enable laser excitation for the transverse array. A unilateral, with respect to the transverse array, placement of the fiberoptic aperture at the tip of the probe with individual fibers oriented in the radial direction may constitute one feasible approach. Additionally, the optoacoustic image reconstruction algorithms used with limited aperture probes perform the best for linear or concave variants of the array (Xu *et al.*, 2004; Modgil and La Riviere, 2009). Optoacoustic images reconstructed with the convex arrays, such as the transverse array in a TRUS probe demonstrated a significant decrease of the image quality (Xu *et al.*, 2004; Yaseen *et al.*, 2010). Another formidable challenge would be to keep the bi-plane probe modified with fiberoptic light delivery for both arrays compact within the major diameter limitations imposed by anthropometric characteristics of the rectum. Finally, the susceptibility of the OA-Tim technique to motion artifacts should be carefully investigated, and registration algorithms developed using anatomical information provided by co-registered ultrasound imaging.

In order to establish a higher level of procedural control, some prototype cryotherapy systems are built to work with magnetic resonance (MR) imaging modalities, which provide non-invasive temperature readouts (Onik, 2001; Sankineni *et al.*, 2014). The most popular investigational MR technique, the proton resonance frequency shift-based MR thermometry (PRFS-MRT), primarily exploits the temperature dependence of the proton resonance frequency in water (Rieke and Butts Pauly, 2008; Yuan *et al.*, 2012). However, it has a poor performance for fatty tissues, and motion-induced image misregistration during successive acquisitions produces a large error in this technique (Jenista *et al.*, 2010; Zou *et al.*, 2013). The accuracy of a recently introduced referenceless MRT technique (Zou *et al.*, 2013) was estimated in experiments on excised tissue samples to be only 4-9 °C. The accuracy of *in vivo* MRT imaging is expected to be even lower. MRT systems are also impractical for monitoring cryotherapy of prostate cancer since they are extremely expensive as compared to the core cryotherapy machine, cannot produce images in real-time, lack portability, and require special MR-compatible facilities and thermal-ablation equipment.

Another investigational approach to non-invasive temperature imaging suggested utilizing the transrectal ultrasound imaging by itself. Ultrasound-based thermometry uses detection of thermally induced mechanical changes in tissue properties such as speed of sound (SOS),

attenuation, and the acoustic nonlinearity parameter (Miller *et al.*, 2002; Damianou *et al.*, 1997). The most commonly implemented ultrasound thermometry approach maps the spatial distribution of the apparent strain caused by thermally induced changes in SOS. However, a temperature change of 10°C results in a <1% change in SOS. Hence, this approach suffers from low and tissue-dependent sensitivity; the behavior of calibration function was also found the opposite for fat-rich tissues and water-rich tissues (Hsiao and Deng, 2016).

Analysis of the precision (random noise) and the single readout accuracy of the temperature imaging technique used in these pilot *in vivo* studies was investigated *in vitro* and discussed in details in our previous publication (Petrova *et al.*, 2016). In those studies, we analyzed 30 independent OA temperature calibration data collected from porcine blood samples. The precision of OA temperature measurements was reported to be ±0.1°C in optically transparent phantoms, which is comparable to that of direct thermocouple readouts employed in clinical cryotherapy. However, the precision reduced about 4 times in optically scattering tissue-mimicking phantoms, and it was attributed to the reduced contrast-to-noise ratio (CNR) of the OA images. We also demonstrated that the accuracy of OA thermometry using our imaging technique (estimated as the 95% prediction interval for a single measurement) could be as high as ±1°C for temperatures below 0°C. The average accuracy estimated for the entire interrogated range of temperatures (40°C to −16°C) was ±3°C.

The precision of OA temperature measurements in our pilot *in vivo* studies was limited by the maximum local cooling rates, which reached 20°C/min near the monitored region of the prostate as measured by the thermocouples Th2 and Th3 (Figure 6(c)). For temperature imaging, we averaged every ten OA image frames, which reduced the random component of the system noise and improved CNR by about 3 times, but simultaneously decreased the monitoring frame rate down to 1 fps. Consequently, the theoretical precision of the OA temperature imaging within the monitored region of the prostate was limited to about ±0.17°C. The observed standard deviation of the optoacoustically mapped temperature from the blood calibration curve was ±2°C for a highly vascularized region (Figure 6(b)), which is adequate for providing clinicians with the required 10°C isotherms. Similar standard deviation numbers can be obtained while analyzing OA data versus the readings of nearby thermocouples (Figure 6(c)). However, since the original blood calibration curve was derived from *in vitro* experiments on a different mammalian species (pig vs dog in the current studies), and considering the large temperature gradients, which were present during cryotherapy, those numbers could serve only for a very rough estimate of the technique's *in vivo* accuracy.

In these feasibility studies, our prototype OA imaging system was not evaluated for the sensitivity and for the noise characteristics. The performance of an optoacoustic detector is frequently quantified using a characteristic called noise-equivalent pressure (NEP), which is calculated as Output noise (volts)/Sensitivity (volts/pascals). The lower the NEP, the better is the detector's performance. However, for an optoacoustic imaging system, such characteristic is incomplete and provides only a glimpse at the quality of the used transducers and analog electronics. Dynamic range, digital resolution of the transducer signals, and the implemented signal conditioning, image reconstruction, and image processing will critically contribute to the resultant quality of the optoacoustic imaging

system. In our previous studies (Petrova *et al.*, 2013), we already showed that image-based OA-Tim has about 10-fold precision advantage as compared to a single-transducer thermometry. In the future, we plan to develop a standard quality assessment procedure and a set of relevant characteristics for the OA-Tim system, and the system will be modified to optimize its temperature imaging performance.

Local pressure change per degree of temperature is defined by the thermal behavior of the Grüneisen parameter and optical absorption coefficient of the erythrocytes, as well as by the locally delivered optical fluence. On a micro-scale it is independent of the blood volume. For example, if the local optical fluence in the monitored vascularized region is 5 mJ/cm^2, optical absorption coefficient of an erythrocyte (5.3 mM Hb) at 805 nm is 10 cm^{-1} (molar extinction of Hb ~800 cm-1/M) (Petrova *et al.*, 2014; Jacques, 2013), and the Grüneisen parameter of an erythrocyte is 0.15 at 22°C (Yao *et al.*, 2014) and zero at −13°C (Petrova *et al.*, 2014), then the local pressure change will be about 200 Pa/°C. However, typical transducers which are used for biomedical optoacoustic imaging beyond microscopy, have high cut-off frequency on the order of 5-10 MHz, and are unable to detect individual red blood cells, but rather produce signals proportional to the optical absorption coefficient averaged over some volume of tissue, and, therefore, proportional to the local volumetric blood content. It would be extremely interesting to investigate how the sensitivity of an OA-Tim system depends on the local blood content of the monitored tissue, whether it is represented by individual blood vessels, which are visible as discrete objects on the optoacoustic images, or by a network of small capillaries, which are manifested through increased levels of OA image background.

Significant spatial heterogeneity of temperature during cryotherapy also translates into the spatial heterogeneity of speed of sound and presents an additional challenge for OA-Tim. If not accounted for, it may lead to defocusing and distortion of the reconstructed optoacoustic images, reducing the accuracy of the temperature maps. A more sophisticated image reconstruction algorithm accounting for the thermally induced spatial variations of speed of sound may improve the robustness of the reconstructed images (Dean-Ben *et al.*, 2014).

The method of OA temperature imaging implemented in these studies relies on the accurate acquisition of the reference frame, which should be established with high averaging prior to initiation of cryotherapy. At normal physiological conditions, tissue temperature is tightly controlled by the regulatory mechanisms, and there are no significant temperature gradients present. Therefore, the temperature within the optoacoustically interrogated field of view could be considered spatially homogeneous. A control temperature needle sensor is still desired to be present during cryotherapy to improve the accuracy of the reference frame and to add extra safety by providing real-time validation of the constructed temperature maps in the specific spatial location within the monitored field of view.

Both precision and accuracy of OA-Tim are significantly affected by the contrast-to-noise ratio of the optoacoustic images. Therefore, it is imperative that the studied live tissue is sufficiently vascularized. The prostate gland does not belong to the category of highly vascularized tissues (see the dissected prostate in Figure 6(d)). Therefore, it is expected that inside the prostate gland the OA-Tim technique will have a significantly reduced accuracy.

One method to improve the accuracy of OA-Tim in the tissues with low blood content is to enhance those by administering an optical contrast agent (Chen *et al.*, 2012; Petrova *et al.*, 2017). One example of such contrast agent is the indocyanine green dye (ICG) approved by the U.S. FDA for use in humans in a form of intravenous injections (Fox and Wood, 1960). Bulk ICG or its compartmentalized forms (Bahmani *et al.*, 2013; Hannah *et al.*, 2014) could be directly injected into the prostate immediately preceding the freezing cycle, significantly increasing its optoacoustic contrast. Following the cryotherapy, the immune system will clear the non-toxic dye along with the damaged prostate tissue.

The universal temperature-dependent OA response in blood is valid only while hemoglobin remains inside erythrocytes (Petrova *et al.*, 2014). Previously, we demonstrated that erythrocytes exposed to the laser radiation that is used to excite optoacoustic response during the OA-Tim remain intact with all the hemoglobin still compartmentalized inside the cytoplasm (Petrova *et al.*, 2016). However, temperatures below −20 °C and the phase transition experienced by tissue inside the ice ball during cryotherapy will produce extended rates of hemolysis (break up of red blood cells). A critical *in vivo* study must then be aimed to the understanding of the role of thermally induced hemolysis and its magnitude during cryotherapy, identifying the regions with minimally damaged blood vessels and erythrocytes, where the universally calibrated ThOR of blood will remain valid and accurate.

When the iceball reaches the optoacoustically monitored region of tissue, the Grüneisen parameter, and consequently the optoacoustic response, abruptly change their signs and magnitude (Larin *et al.*, 2002). The calibration equation (Eq. 1) becomes no longer valid. Additionally, the acoustic heterogeneity in the mixture of frozen/non-frozen tissue will decrease the quality of reconstructed OA frames and the accuracy of OA temperature imaging. Our previous studies (Petrova *et al.*, 2016) demonstrated that high-contrast optoacoustic sources, like blood vessels, become blurred and ultimately invisible once they are inside the iceball. We considered all those difficulties and limitations and proposed to use the OA temperature imaging technique for monitoring only vascularized non-frozen tissue around the rectal wall, just before the ice ball propagates to that region. However, the ultrasound image in Figure 5(b) shows that by the end of the freezing cycle the iceball propagated into the optoacoustically monitored region. Therefore, some frames just before the freezing were stopped and soon thereafter will contain valid temperature maps only up to the depth of 7.5 mm. At the same time, the vascularized region used for validation of OA temperature readings was located at a depth of 5 mm (Figure 6(b)) and was not affected by the iceball providing a valid reference point for the technique. Also, the temperature data logged by the thermocouples Th2 and Th3, which served as control references did not drop below −17°C (Figure 6(c)), indicating that the surrounding tissue should have remained non-frozen.

During *in vivo* optoacoustic monitoring of cryotherapy, we also observed a peculiar phenomenon, which might be related to a physiological response of the thermoregulatory system during the initial phase of the freezing cycle. Figure 6(b) shows the dramatic 2× increase in the normalized optoacoustic image intensity in the early phase of the freezing, while the nearby thermocouples were still logging constant temperature. A live organism has a remarkable capacity for maintaining local temperatures via thermoregulatory mechanisms

(Schonbaum and Lomax, 1991). One of the core mechanisms involves temporary redistribution of blood perfusion as the arterioles and vascular bypasses are opened or closed in response to the local temperature changes by contraction of smooth muscle cells in their walls. We suggest that the following mechanism could explain the phenomenon of increased optoacoustic response, which is clearly visible in Figure 6(b) during the first 60 seconds of freezing. After the freezing of the prostate is initiated and the cool front reaches the monitored vascularized areas in the Denonvilliers fascia and rectal wall, local vasodilation momentarily decreases vascular resistance in an attempt to compensate the heat losses by the increased influx of the warm blood from outside of the thermally treated area. The increase in the local blood perfusion increases average optical absorption coefficient of that region resulting in a proportional growth of the optoacoustic response. However, at some point, the vascular thermoregulatory mechanisms become overwhelmed by the power of the freezing source, the temperatures inside the blood vessels and capillaries drop further, leading to decrease in blood viscosity, reduction of the flow rate, and, eventually, to local thrombosis. Red blood cells stop moving, and the relationship between normalized optoacoustic response and temperature returns back to that observed *in vitro* (Figure 6(b) below 20-30°C). Cold-induced local damage to blood vessels is known to be one of the earliest biological effects of cryotherapy (Figure 1), causing platelet activation and thrombosis (Theodorescu, 2004; Mohammed *et al.*, 2014). Since the thermoregulatory compensation happens early during the freezing cycle enhancing the local blood flow, it should not significantly affect the accuracy of OA-Tim in the critical temperature range around 0°C and below, until the ice crystals begin forming in blood at about −20°C. This phenomenon may be further investigated by studying the changes of local tissue perfusion during OA temperature imaging using the ultrasound Doppler, which is readily available in any clinical cryotherapy system. It should provide crucial answers on how and when the reference OA frame should be selected to keep the temperature imaging technique valid during most important phases of cryotherapy.

Conclusion

The presented *in vivo* results showed that the OA temperature imaging is a promising noninvasive technique for real-time imaging of tissue temperature during cryotherapy of prostate cancer, which can be combined with the current standard for guiding clinical cryotherapy procedure – the transrectal ultrasound. However, enabling clinical application of the OA temperature imaging still requires some significant research and development efforts, including investigation of the physiologic thermoregulatory mechanisms and their impact on the accuracy of the technique, susceptibility to motion artifacts, inter-frame registration, and probe design optimized for use in humans.

Acknowledgments

This work was supported in part by the National Cancer Institute, NIH grant R43CA177148. AAO acknowledges financial support by Guangdong Health and Family Planning Commission of Guangzhou Municipality, Project No. 20161A011092. The free loan of the Cryocare® CS system was provided by HealthTronics, Austin, Texas.

References

Agarwal PK, Sadetsky N, Konety BR, Resnick MI, Carroll PR, Cancer of the Prostate Strategic Urological Research E. Treatment failure after primary and salvage therapy for prostate cancer: likelihood, patterns of care, and outcomes. Cancer. 2008; 112:307–14. [PubMed: 18050294]

ANSI. Americal National Standard for Safe Use of Lasers. Americal National Standards Institutes. 2007; Z136.1:6–24.

Bahmani B, Bacon D, Anvari B. Erythrocyte-derived photo-theranostic agents: hybrid nano-vesicles containing indocyanine green for near-infrared imaging and therapeutic applications. Sci Rep. 2013; 3:2180. [PubMed: 23846447]

Bjerklund Johansen TE, Witzsch U, Greene D. Salvage treatment in prostate cancer: a clinical approach. Expert review of anticancer therapy. 2013; 13:613–23. [PubMed: 23617352]

Chen YS, Frey W, Aglyamov S, Emelianov S. Environment-dependent generation of photoacoustic waves from plasmonic nanoparticles. Small (Weinheim an der Bergstrasse, Germany). 2012; 8:47–52.

Chen YS, Frey W, Walker C, Aglyamov S, Emelianov S. Sensitivity enhanced nanothermal sensors for photoacoustic temperature mapping. J Biophotonics. 2013; 6:534–42. [PubMed: 23450812]

Chu KF, Dupuy DE. Thermal ablation of tumours: biological mechanisms and advances in therapy. Nat Rev Cancer. 2014; 14:199–208. [PubMed: 24561446]

Damianou CA, Sanghvi NT, Fry FJ, Maass-Moreno R. Dependence of ultrasonic attenuation and absorption in dog soft tissues on temperature and thermal dose. The Journal of the Acoustical Society of America. 1997; 102:628–34. [PubMed: 9228822]

Dean-Ben XL, Ntziachristos V, Razansky D. Effects of small variations of speed of sound in optoacoustic tomographic imaging. Med Phys. 2014; 41:073301. [PubMed: 24989414]

Durand M, Barret E, Galiano M, Rozet F, Sanchez-Salas R, Ahallal Y, Macek P, Gaya JM, Cerruti J, Devilliers H, Loeffler J, Amiel J, Vallancien G, Cathelineau X. Focal cryoablation: a treatment option for unilateral low-risk prostate cancer. BJU international. 2014; 113:56–64. [PubMed: 24053685]

Ermilov SA, Khamapirad T, Conjusteau A, Leonard MH, Lacewell R, Mehta K, Miller T, Oraevsky AA. Laser optoacoustic imaging system for detection of breast cancer. J Biomed Opt. 2009; 14:024007. [PubMed: 19405737]

Esenaliev R, Larina I, Larin K, Motamedi M. Real-time optoacoustic monitoring during thermotherapy. Proceedings SPIE. 2000; 3916:302–10.

Esenaliev RO, Oraevsky AA, Larin KV, Larina IV, Motamedi M. Real-time optoacoustic monitoring of temperature in tissues. Proc SPIE. 1999; 3601:268–75.

Fonseca-Alves CE, Vicente IST, Calazans SG, Laufer-Amorim R. Canine prostate cancer: Would the dog be an important model for the study of new drugs? American Journal of Drug Discovery and Development. 2013; 3:220–4.

Fox IJ, Wood EH. Indocyanine green: physical and physiologic properties. Proceedings of the staff meetings Mayo Clinic. 1960; 35:732–44. [PubMed: 13701100]

Fronheiser MP, Ermilov SA, Brecht HP, Conjusteau A, Su R, Mehta K, Oraevsky AA. Real-time optoacoustic monitoring and three-dimensional mapping of a human arm vasculature. J Biomed Opt. 2010; 15

Garnick MB. Prostate cancer: screening, diagnosis, and management. Annals of internal medicine. 1993; 118:804–18. [PubMed: 7682387]

Hannah A, Luke G, Wilson K, Homan K, Emelianov S. Indocyanine green-loaded photoacoustic nanodroplets: dual contrast nanoconstructs for enhanced photoacoustic and ultrasound imaging. ACS Nano. 2014; 8:250–9. [PubMed: 24303934]

Harrison T, Zemp RJ. Coregistered photoacoustic-ultrasound imaging applied to brachytherapy. J Biomed Opt. 2011; 16:080502. [PubMed: 21895302]

Howlader, N., Noone, AM., Krapcho, M., Miller, D., Bishop, K., Kosary, CL., Yu, M., Ruhl, J., Tatalovich, Z., Mariotto, A., Lewis, DR., Chen, HS., Feuer, EJ., Cronin, KA. SEER Cancer Statistics Review, 1975–2014. Bethesda, MD: National Cancer Institute; 2017.

Hsiao YS, Deng CX. Calibration and Evaluation of Ultrasound Thermography Using Infrared Imaging. Ultrasound in medicine & biology. 2016; 42:503–17. [PubMed: 26547634]

Ismail M, Ahmed S, Kastner C, Davies J. Salvage cryotherapy for recurrent prostate cancer after radiation failure: a prospective case series of the first 100 patients. BJU international. 2007; 100:760–4. [PubMed: 17662081]

Jacques SL. Optical properties of biological tissues: a review. Phys Med Biol. 2013; 58:R37–61. [PubMed: 23666068]

Jaeger M, Bamber JC, Frenz M. Clutter elimination for deep clinical optoacoustic imaging using localized vibration tagging (LOVIT). Photoacoustics. 2013; 1:19–29. [PubMed: 25302147]

Jenista ER, Branca RT, Warren WS. Absolute temperature imaging using intermolecular multiple quantum MRI. Int J Hyperthermia. 2010; 26:725–34. [PubMed: 20849265]

Jones JS, Rewcastle JC, Donnelly BJ, Lugnani FM, Pisters LL, Katz AE. Whole gland primary prostate cryoablation: initial results from the cryo on-line data registry. The Journal of urology. 2008; 180:554–8. [PubMed: 18550117]

Ke H, Tai S, Wang LV. Photoacoustic thermography of tissue. J Biomed Opt. 2014; 19:26003.

Kruger RA, Liu P, Fang YR, Appledorn CR. Photoacoustic ultrasound (PAUS)–reconstruction tomography. Med Phys. 1995; 22:1605–9. [PubMed: 8551984]

Larin K, Larina I, Motamedi M, Esenaliev R. Monitoring of temperature distribution in tissues with optoacoustic technique in real time. Proc SPIE. 2000; 3916:311–21.

Larin KV, Larina IV, Motamedi M, Esenaliev RO. Optoacoustic laser monitoring of cooling and freezing of tissues. Quantum Electronics. 2002; 32:953–8.

Larina IV, Larin KV, Esenaliev RO. Real-time optoacoustic monitoring of temperature in tissues. J Phys D. 2005; 38:2633–9.

Maytal, BZ. Advances in Cryogenic Engineering. Kittel, P., editor. New York: Springer US; 1998. p. 911-7.

Miller NR, Bamber JC, Meaney PM. Fundamental limitations of noninvasive temperature imaging by means of ultrasound echo strain estimation. Ultrasound in medicine & biology. 2002; 28:1319–33. [PubMed: 12467859]

Modgil D, La Riviere PJ. Implementation and comparison of reconstruction algorithms for two-dimensional optoacoustic tomography using a linear array. J Biomed Opt. 2009; 14:044023. [PubMed: 19725734]

Mohammed A, Miller S, Douglas-Moore J, Miller M. Cryotherapy and its applications in the management of urologic malignancies: a review of its use in prostate and renal cancers. Urol Oncol. 2014; 32:39 e19–27.

Neuschler EI, Butler R, Young CA, Barke LD, Bertrand ML, Bohm-Velez M, Destounis S, Donlan P, Grobmyer SR, Katzen J, Kist KA, Lavin PT, Makariou EV, Parris TM, Schilling KJ, Tucker FL, Dogan BE. A Pivotal Study of Optoacoustic Imaging to Diagnose Benign and Malignant Breast Masses: A New Evaluation Tool for Radiologists. Radiology. 2017:172228. [PubMed: 29178816]

Nguyen HD, Allen BJ, Pow-Sang JM. Focal cryotherapy in the treatment of localized prostate cancer. Cancer control: journal of the Moffitt Cancer Center. 2013; 20:177–80. [PubMed: 23811701]

Nikitin SM, Khokhlova TD, Pelivanov IM. Temperature dependence of the optoacoustic transformation efficiency in ex vivo tissues for application in monitoring thermal therapies. J Biomed Opt. 2012; 17:061214. [PubMed: 22734744]

Onik G. Image-guided prostate cryosurgery: state of the art. Cancer control: journal of the Moffitt Cancer Center. 2001; 8:522–31. [PubMed: 11807422]

Oraevsky, AA. Biomedical photonics handbook. Vo-Dinh, T., editor. Boca Raton: CRC Press; 2014. p. 715-57.

Petrova E, Ermilov S, Su R, Nadvoretskiy V, Conjusteau A, Oraevsky A. Using optoacoustic imaging for measuring the temperature dependence of Gruneisen parameter in optically absorbing solutions. Opt Express. 2013; 21:25077–90. [PubMed: 24150350]

Petrova E, Liopo A, Nadvoretskiy V, Ermilov S. Imaging technique for real-time temperature monitoring during cryotherapy of lesions. J Biomed Opt. 2016; 21:116007. [PubMed: 27822579]

Petrova E, Liopo A, Oraevsky AA, Ermilov SA. Temperature-dependent optoacoustic response and transient through zero Gruneisen parameter in optically contrasted media. Photoacoustics. 2017; 7:36–46. [PubMed: 28725558]

Petrova EV, Oraevsky AA, Ermilov SA. Red blood cell as a universal optoacoustic sensor for non-invasive temperature monitoring. Appl Phys Lett. 2014; 105:094103. [PubMed: 25316928]

Pramanik M, Wang LV. Thermoacoustic and photoacoustic sensing of temperature. J Biomed Opt. 2009; 14

Resnick MJ, Koyama T, Fan KH, Albertsen PC, Goodman M, Hamilton AS, Hoffman RM, Potosky AL, Stanford JL, Stroup AM, Van Horn RL, Penson DF. Long-term functional outcomes after treatment for localized prostate cancer. The New England journal of medicine. 2013; 368:436–45. [PubMed: 23363497]

Rieke V, Butts Pauly K. MR thermometry. Journal of magnetic resonance imaging: JMRI. 2008; 27:376–90. [PubMed: 18219673]

Roberts CB, Jang TL, Shao YH, Kabadi S, Moore DF, Lu-Yao GL. Treatment profile and complications associated with cryotherapy for localized prostate cancer: a population-based study. Prostate Cancer Prostatic Dis. 2011; 14:313–9. [PubMed: 21519347]

Robilotto AT, Baust JM, Van Buskirk RG, Gage AA, Baust JG. Temperature-dependent activation of differential apoptotic pathways during cryoablation in a human prostate cancer model. Prostate Cancer Prostatic Dis. 2013; 16:41–9. [PubMed: 23229563]

Rukstalis, D., Katz, AE. Handbook of urologic cryoablation. New York: Informa Healthcare; 2007.

Sankineni S, Wood BJ, Rais-Bahrami S, Walton Diaz A, Hoang AN, Pinto PA, Choyke PL, Turkbey B. Image-guided focal therapy for prostate cancer. Diagnostic and interventional radiology. 2014; 20:492–7. [PubMed: 25205025]

Schonbaum, L., Lomax, P. Thermoregulation: Physiology and Biochemistry. Oxford; Pergamon: 1991.

Soroushian B, Whelan WM, Kolios MC. Study of laser-induced thermoelastic deformation of native and coagulated ex-vivo bovine liver tissues for estimating their optical and thermomechanical properties. J Biomed Opt. 2010; 15:065002. [PubMed: 21198166]

Theodorescu D. Cancer cryotherapy: evolution and biology. Rev Urol. 2004; 6(Suppl 4):S9–S19.

Wang B, Emelianov S. Thermal intravascular photoacoustic imaging. Biomedical optics express. 2011; 2:3072–8. [PubMed: 22076268]

Wang LV, Hu S. Photoacoustic tomography: in vivo imaging from organelles to organs. Science. 2012; 335:1458–62. [PubMed: 22442475]

Williams AK, Martinez CH, Lu C, Ng CK, Pautler SE, Chin JL. Disease-free survival following salvage cryotherapy for biopsy-proven radio-recurrent prostate cancer. European urology. 2011; 60:405–10. [PubMed: 21185115]

Xu Y, Wang LV, Ambartsoumian G, Kuchment P. Reconstructions in limited-view thermoacoustic tomography. Med Phys. 2004; 31:724–33. [PubMed: 15124989]

Yao DK, Zhang C, Maslov K, Wang LV. Photoacoustic measurement of the Gruneisen parameter of tissue. J Biomed Opt. 2014; 19

Yaseen MA, Ermilov SA, Brecht HP, Su R, Conjusteau A, Fronheiser M, Bell BA, Motamedi M, Oraevsky AA. Optoacoustic imaging of the prostate: development toward image-guided biopsy. J Biomed Opt. 2010; 15

Yuan J, Mei CS, Panych LP, McDannold NJ, Madore B. Towards fast and accurate temperature mapping with proton resonance frequency-based MR thermometry. Quantitative imaging in medicine and surgery. 2012; 2:21–32. [PubMed: 22773966]

Zisman A, Pantuck AJ, Cohen JK, Belldegrun AS. Prostate cryoablation using direct transperineal placement of ultrathin probes through a 17-gauge brachytherapy template-technique and preliminary results. Urology. 2001; 58:988–93. [PubMed: 11744474]

Zou C, Shen H, He M, Tie C, Chung YC, Liu X. A fast referenceless PRFS-based MR thermometry by phase finite difference. Phys Med Biol. 2013; 58:5735–51. [PubMed: 23902944]

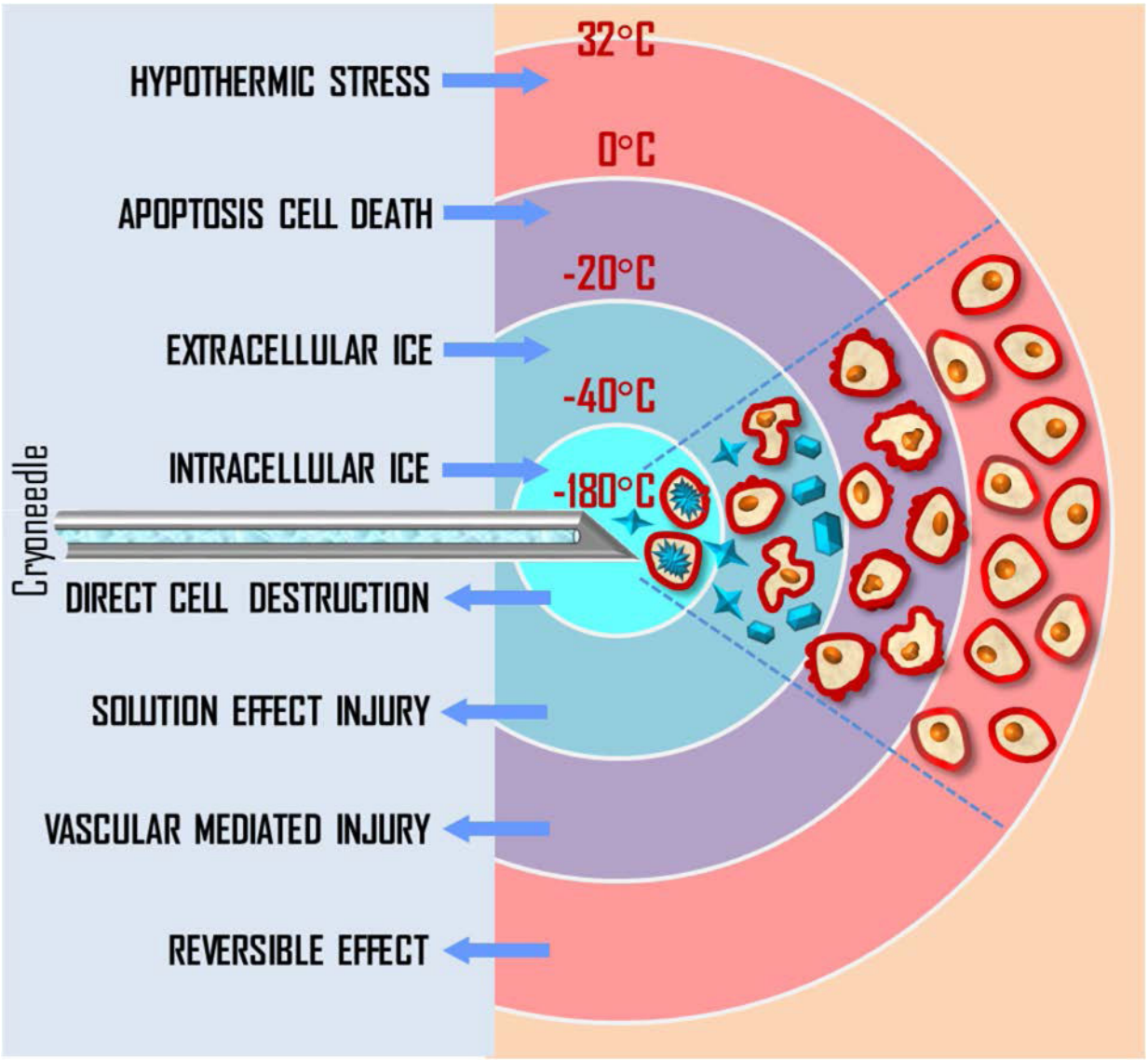

Figure 1.
Biological effects of cryotherapy.

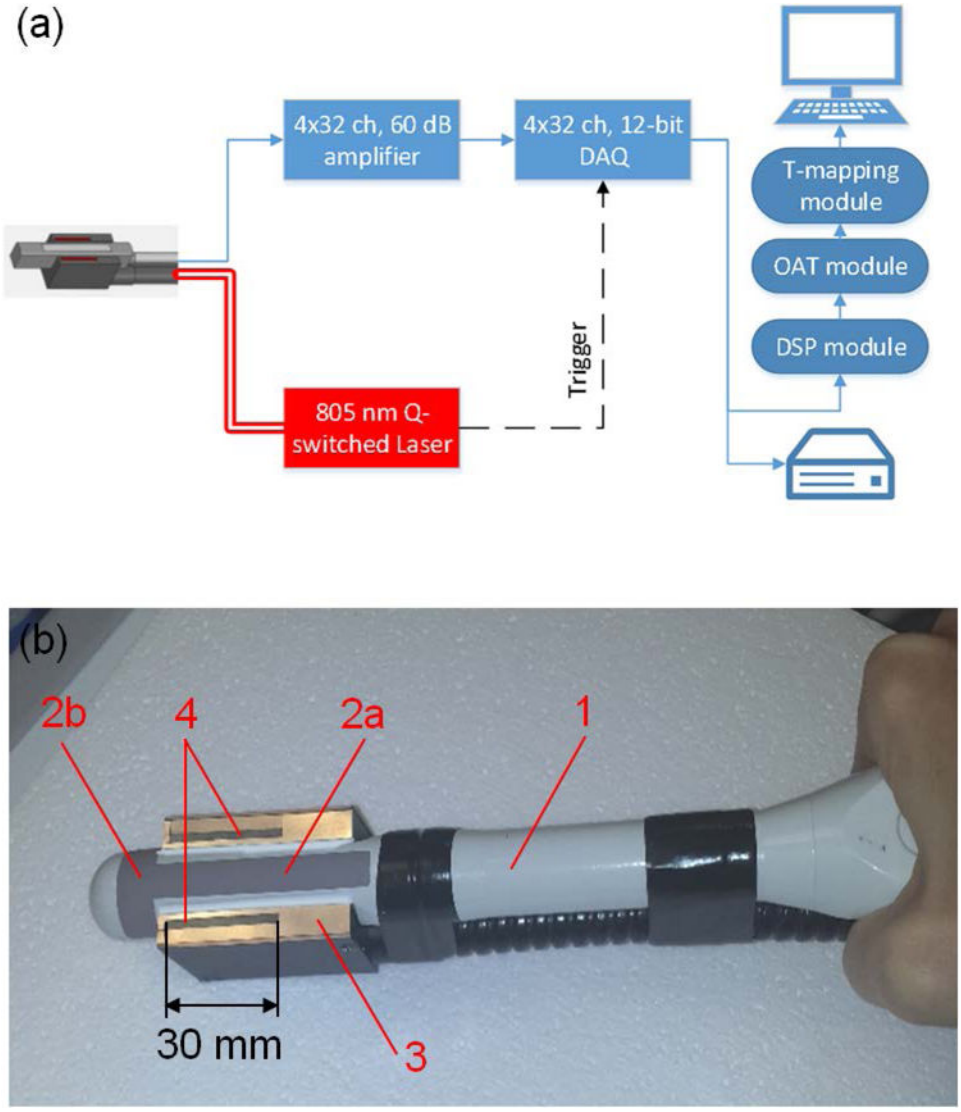

Figure 2.

(a) Schematic of the optoacoustic thermometry prototype for monitoring cryotherapy of prostate. DAQ – data acquisition, DSP – digital signal processing, OAT – optoacoustic tomography, T-mapping – temperature imaging. (b) Transrectal ultrasound (TRUS) probe (1) incorporates two orthogonal arrays of transducers: longitudinal (2a) and transverse (2b); the output terminal of the fiberoptic bundle (3) enables longitudinal optoacoustic view of the prostate excited by 805-nm laser pulses through the light-emitting apertures (4).

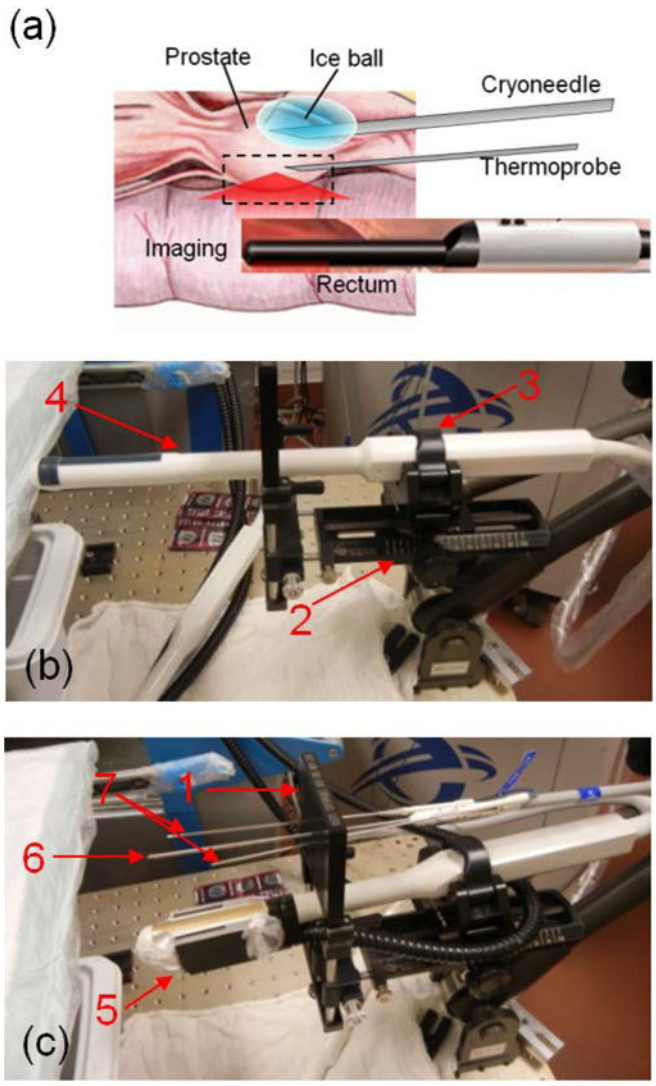

Figure 3.

(a) Schematic showing *in vivo* optoacoustic temperature monitoring during cryotherapy of the canine prostate. Photographs show settings with transrectal probes for ultrasound imaging (b) and optoacoustic thermometry (c). 1 – CryoGrid™ fixture; 2 – probe holder; 3 – quick-latch; 4 – transrectal ultrasound (TRUS) probe; 5 – optoacoustic thermometry probe; 6 – cryoneedle; 7 – thermal sensors (thermoprobes).

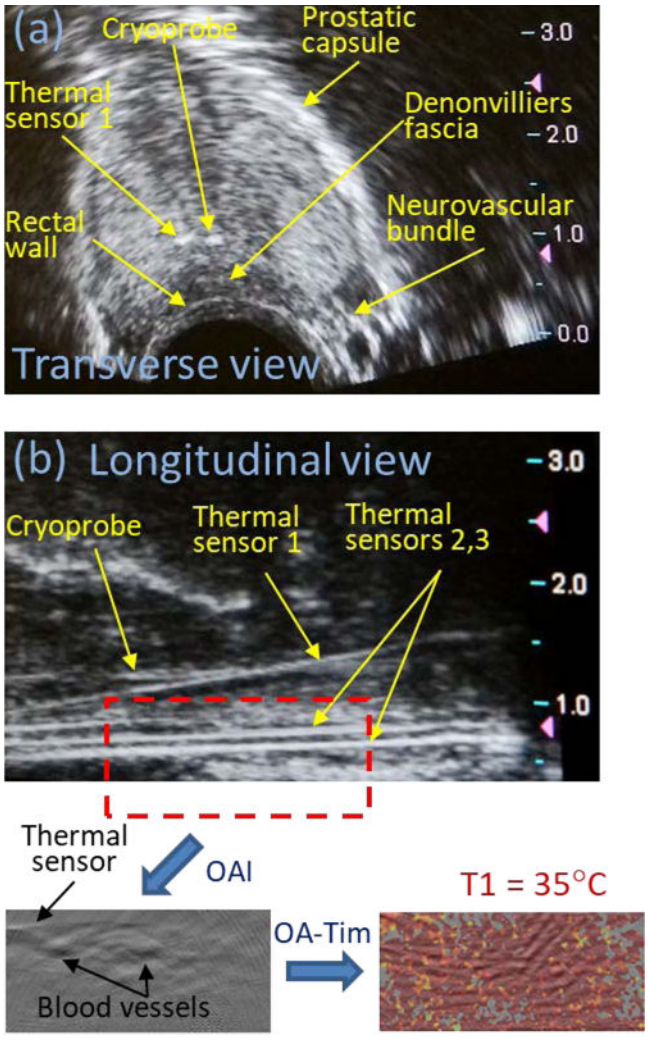

Figure 4.

(a) Transverse and (b) longitudinal ultrasound images of a dog's prostate prior to initiation of cryotherapy. Red dashed rectangle on the panel (b) indicates the area that included rectal wall and Denonvilliers fascia, which was used for construction of optoacoustic temperature maps. OAI – optoacoustic imaging; OA-Tim – optoacoustic temperature imaging; T1 – initial temperature of the monitored prostate tissue.

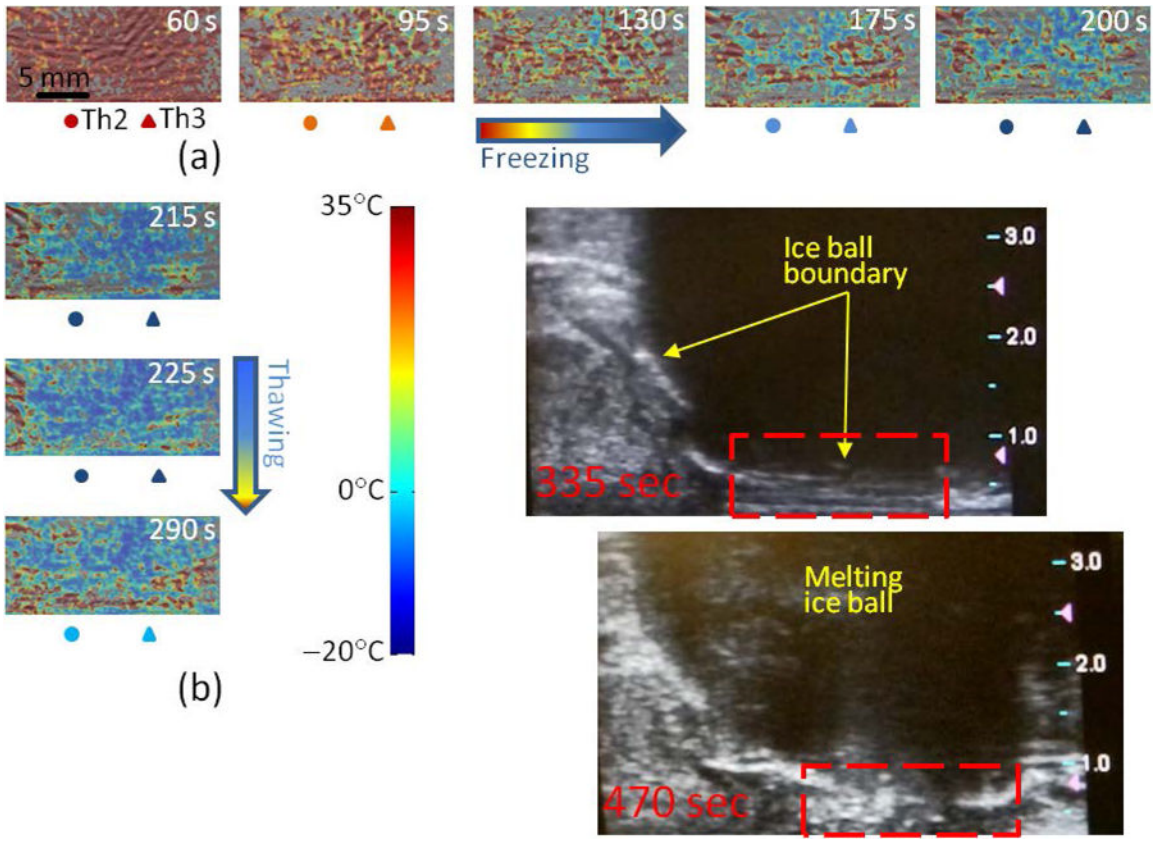

Figure 5.

In vivo optoacoustic imaging of temperature in the area near the rectal wall and Denonvilliers fascia during the freezing (a) and passive thawing (b) cycles of prostate cryotherapy. The timestamp indicates the moment of the frame's acquisition after the initiation of the freezing cycle. The temperatures logged by the thermal sensors Th2 and Th3 set in the Denonvilliers fascia are indicated for each frame in the color code according to the shown color palette. Panel (b) also shows longitudinal ultrasound images of the dog's prostate immediately after the cryotherapy. Ice ball is clearly visible as a large hypoechoic mass. Red dashed rectangle indicates the optoacoustically monitored region of interest.

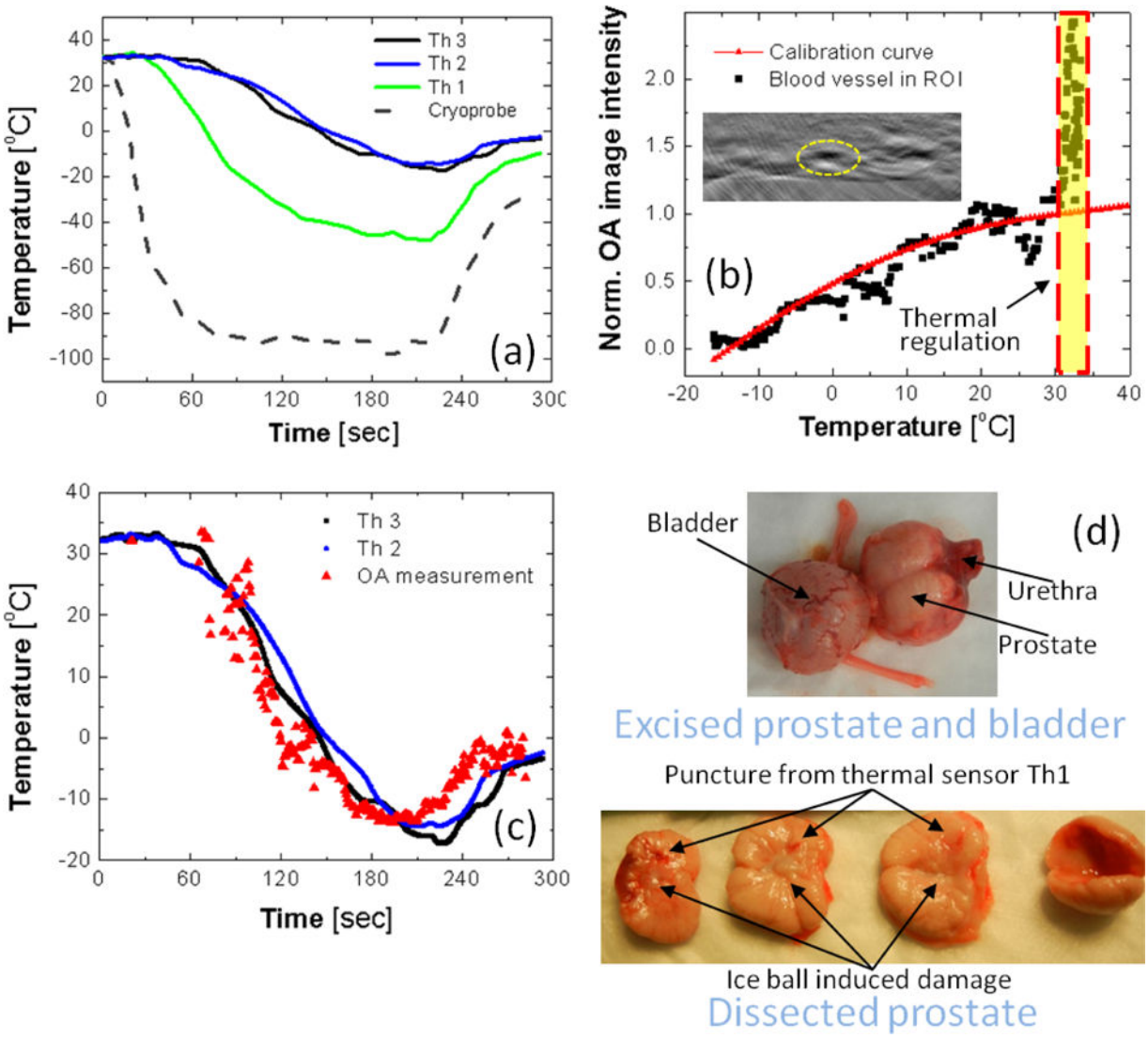

Figure 6.

(a) The temporal temperature profiles recorded by a thermocouple inside the cryoprobe and by three thermal sensors set inside (Th1) and nearby (Th2 and Th3) the prostate treated with cryotherapy. (b) Normalized optoacoustic image intensity of the high-contrast object (blood vessel) inside the region of interest (ROI) shown on the inset as a function of average temperature recorded by nearby thermal sensors Th2 and Th3; For comparison, the *in vitro* obtained universal calibration curve of blood is shown by the red solid line. (c) The temporal temperature profile reconstructed for the object in ROI shown on the panel (b); for comparison, the temporal temperature profiles logged by the nearby thermal sensors Th2 and Th3 are shown by the black and blue solid lines. (d) The dog's prostate was excised and dissected following the cryotherapy to show transverse sections across the urethra demonstrating damage induced by the freezing.